Transport in Porous Media **39:** 97–117, 2000.

Transient Free Convection from a Horizontal Surface in a Porous Medium Subjected to a Sudden Change in Surface Heat Flux

S. D. HARRIS[1], D. B. INGHAM[2] and I. POP[3]
[1]*Rock Deformation Research, School of Earth Sciences, University of Leeds, Leeds LS2 9JT, U.K.*
[2]*Department of Applied Mathematics, University of Leeds, Leeds LS2 9JT, U.K.*
[3]*Faculty of Mathematics, University of Cluj, R-3400 Cluj, CP 253, Romania*

(Received: 11 September 1998; in final form: 22 January 1999)

Abstract. This paper presents an analytical and numerical study of transient free convection from a horizontal surface that is embedded in a fluid-saturated porous medium. It is assumed that for time $\bar{\tau} < 0$ steady state velocity and temperature fields are obtained in the boundary-layer which occurs due to a uniform flux dissipation rate q_1'' on the surface. Then, at $\bar{\tau} = 0$ the heat flux on the surface is suddenly changed to q_2'' and maintained at this value for $\bar{\tau} > 0$. Firstly, solutions which are valid for small and large $\bar{\tau}$ are obtained. The full boundary-layer equations are then integrated step-by-step for the transient regime from the initial unsteady state ($\bar{\tau} = 0$) until such times at which this forward marching approach is no longer well posed. Beyond this time no valid solutions could be obtained which matched the final solution from the forward integration to the steady state profiles at large times $\bar{\tau} \to \infty$.

Key words: free convection, boundary-layer, horizontal surface, transient, heat flux.

Nomenclature

k	effective thermal conductivity.
K	permeability of the porous medium.
q_1''	initial uniform surface heat flux ($\tau < 0$).
q_2''	final uniform surface heat flux ($\tau \geqslant 0$).
R	ratio of the final surface heat flux to the initial surface heat flux, $= q_2''/q_1''$.
Ra_x	local Rayleigh number based on the initial heat flux q_1'', $= g\beta K q_1'' x^2/k\alpha\nu$.
T	fluid temperature.
T_∞	ambient fluid temperature.
ΔT	characteristic temperature, $= q_1''\delta(x)/k$.
u, v	seepage velocity components along x- and y-directions, respectively.
U_c	characteristic velocity, $= (\alpha/x)(\mathrm{Ra}_x)^{1/2}$.
x, y	Cartesian coordinates along the surface and normal to it, respectively.

Greek symbols

α	effective thermal diffusivity.
β	volumetric coefficient of thermal expansion.
δ	boundary-layer thickness at $\bar{\tau} = 0$, $= x(4/\mathrm{Ra}_x)^{1/4}$.

η nondimensional similarity variable, $= y/\delta(x)$.
θ nondimensional temperature function, $= (T - T_\infty)/\Delta T$.
ν kinematic viscosity.
ξ nondimensional transformed variable, $= \eta/2\tau^{1/2}$.
σ ratio of composite material heat capacity to convective fluid heat capacity.
$\bar{\tau}$ time.
τ nondimensional time, $= \alpha\bar{\tau}/\sigma(\delta(x))^2$.
ψ streamfunction.

Subscript
w conditions at the horizontal surface.

1. Introduction

Convective heat transfer in porous media has received considerable attention in recent years owing to its importance in various technological applications such as geothermal systems, grain storage, fibre and granular insulation, electronic system cooling, storage of agricultural products, chemical catalytic reactors, underground diffusion of contaminants, coal combustors and porous material regenerative heat exchangers. Recent books by Nield and Bejan (1999), Nakayama (1995) and Ingham and Pop (1998) excellently describe the extent of the research information in this area.

It has been established that the convection from vertical and horizontal surfaces in a viscous fluid and in a fluid-saturated porous medium have much in common. However, buoyancy induced flows adjacent to horizontal or nearly horizontal surfaces embedded in porous media have not been studied as extensively as those adjacent to vertical surfaces, despite their important applications both in the environment and in technology. In contrast to the vertical surface, where the component of the buoyancy force normal to the surface (i.e. normal to the main flow direction) is neglected, and only its tangential component is considered, this approximation breaks down when the surface becomes horizontal and the buoyancy force acts perpendicular to the surface. When the temperature of a horizontal surface differs from that of the ambient fluid, a vertical density gradient will be generated, indicating a longitudinal pressure gradient. If the resulting longitudinal pressure gradient is large enough to overcome the upward directing buoyancy force, a convective movement will be set up over the horizontal surface, resulting in a horizontal boundary-layer flow.

Steady free convection boundary-layer flow in a porous medium above a heated horizontal surface or below a cooled horizontal surface was first considered by Cheng and Chang (1976) and Chang and Cheng (1983), and their analyses have been very much refined and generalised since then. Recently, Merkin and Zhang (1990), Nakayama (1995), Higuera and Weidman (1995), Lesnic *et al.* (1995), Chaudhary *et al.* (1996), Rees (1996) and Higuera (1997) have published very detailed analytical and numerical solutions for this type of problem.

Most of the recent investigations into boundary-layer flows over a horizontal surface immersed in a porous medium have been directed towards the problem of steady state free or mixed convection flow. Transient boundary-layer flow problems on horizontal surfaces in porous media, on the other hand, have received relatively little attention, so far. Perhaps, the first study on this problem was done by Johnson and Cheng (1978), where similarity solutions were found for certain variations of the wall temperature distribution. Pop and Cheng (1983) exploited the method of integral solutions to attack the problem of transient free convection on a suddenly heated horizontal surface in a porous medium. Ingham *et al.* (1985) used the asymptotic expansion method to study the case of a suddenly cooled horizontal surface embedded in a porous medium.

It is worth mentioning here that the inclusion of unsteadiness into the governing equations of any problem is important for the development of a more physically realistic characterisation of the flow configuration. It is this approach that will provide the best opportunity to discover new kinds of evolutions such as critical situations, instabilities or chaotic structures governed by time-dependent boundary conditions, especially in the cases where velocity and temperature fields are coupled, that is convective flow problems. Moreover, time is a fundamental parameter in many practical situations at a variety of scales, for example in regulation systems as well as in nuclear plant safety or in meteorology.

The present paper is concerned with the transient free convection boundary-layer flow over a horizontal surface embedded in a fluid-saturated porous medium of constant ambient temperature. Thus, we discuss the practical situation in which the general transient arises from a sudden change in the level of energy input flux on the surface of the plate, that is a steady input heat flux q_1'' is changed at the time $\bar{\tau} = 0$ to a new steady level q_2'' and maintained at this value for $\bar{\tau} > 0$. A thin inner boundary-layer is thus formed adjacent to the surface at small times. An analytical solution is given for the velocity and temperature fields in this inner layer using an asymptotic method, which is similar to that employed by Ingham *et al.* (1985). However, the present generalisation and transformed equations are different, since the surface heat flux condition on the plate has been imposed. Then, a numerical step-by-step approach is utilised to derive a solution of the full boundary-layer equations for the transient regime from the initial unsteady state ($\bar{\tau} = 0$) until such times at which this forward integrating approach is no longer well posed. The methods used are similar to that successfully employed by the present authors Harris *et al.* (1996, 1997a, b, 1998) for the corresponding vertical configuration. Beyond the time at which the forward marching approach terminates, various methods have been used in an attempt to match the final profiles of the temperature and streamfunction to their large time steady state solutions. A detailed discussion of the failure of such methods for this problem is also presented. The valid solutions obtained provide a qualitative picture of the nondimensional velocity and temperature fields in the boundary-layer as well as the nondimensional

surface temperature distribution. No doubt, these solutions are relevant to a proper understanding of the general flow and heat transfer characteristics in porous media.

2. Governing Equations

Consider the problem of transient free convection above a horizontal impermeable flat surface which is embedded in a fluid-saturated porous medium of ambient temperature T_∞. We take Cartesian coordinates fixed in space with the x-axis along the horizontal surface and the y-axis normal to it. The y-axis is oriented upwards, while the gravitational acceleration acts vertically downwards. The initial steady situation is that of two-dimensional free convection due to a uniform heat flux dissipation rate q_1'' at the surface. A transient begins when the heat flux on the plate is suddenly changed at time $\bar{\tau} = 0$ to q_2'' and maintained at this value for $\bar{\tau} > 0$. In the mathematical formulation of the problem, we assume that the Darcy–Boussinesq approximation is valid. With the further assumption that the Rayleigh number is large so that the boundary-layer approximation can be applied, the governing equations for the transient response are (see Nield and Bejan, 1999)

$$\frac{\partial u}{\partial x} + \frac{\partial v}{\partial y} = 0, \tag{1}$$

$$\frac{\partial u}{\partial y} = -\frac{g\beta K}{\nu}\frac{\partial T}{\partial x}, \tag{2}$$

$$\sigma\frac{\partial T}{\partial \bar{\tau}} + u\frac{\partial T}{\partial x} + v\frac{\partial T}{\partial y} = \alpha\frac{\partial^2 T}{\partial y^2}, \tag{3}$$

for $\bar{\tau} > 0$. Here $u(x, y, \bar{\tau})$ and $v(x, y, \bar{\tau})$ denote the seepage velocity components along the x- and y-directions, respectively, $T(x, y, \bar{\tau})$ is the fluid temperature, g is the magnitude of the acceleration due to gravity, K is the permeability of the porous medium, σ is the heat capacity ratio, ν is the kinematic viscosity, β is the volumetric coefficient of thermal expansion and α is the effective thermal diffusivity of the fluid-saturated porous medium.

For time $\bar{\tau} < 0$, the steady flow results from the uniform surface heat flux q_1'', while for $\bar{\tau} \geqslant 0$ the transient flow is a consequence of the uniform heat flux q_2''. Thus, the governing boundary-layer Equations (1)–(3) must be solved subject to the following boundary conditions:

$$\begin{aligned} &u(x, \infty, \bar{\tau}) = 0, \quad T(x, \infty, \bar{\tau}) = T_\infty, \\ &v(x, 0, \bar{\tau}) = 0, \quad \frac{\partial T}{\partial y}(x, 0, \bar{\tau}) = -\frac{q_2''}{k}, \end{aligned} \tag{4}$$

where k is the effective thermal conductivity.

For $\bar{\tau} \geqslant 0$, we now introduce the time-dependent, nondimensional, reduced streamfunction, f, and the temperature function, θ, defined according to

$$\psi = U_c \delta(x) f(\eta, \tau), \quad \theta(\eta, \tau) = \frac{T - T_\infty}{\Delta T}, \tag{5}$$

where

$$\begin{aligned} &\eta = \frac{y}{\delta(x)}, \quad \tau = \frac{\alpha \bar{\tau}}{\sigma(\delta(x))^2}, \quad \delta(x) = x\left(\frac{4}{\mathrm{Ra}_x}\right)^{1/4}, \\ &U_c = \frac{\alpha}{x}(\mathrm{Ra}_x)^{1/2} = \left(\frac{\alpha g \beta K q_1''}{k\nu}\right)^{1/2}, \\ &\Delta T = \frac{q_1'' \delta(x)}{k}, \quad \mathrm{Ra}_x = \frac{g\beta K q_1'' x^2}{k\alpha\nu}. \end{aligned} \tag{6}$$

Further, η is the nondimensional similarity variable, τ is the nondimensional time, $\delta(x)$ is the boundary-layer thickness at $\bar{\tau} = 0$, U_c is the characteristic velocity, ΔT is the characteristic temperature, Ra_x is the local Rayleigh number based on the initial heat flux q_1'' and ψ is the streamfunction which is defined in the usual way, namely $u = \partial\psi/\partial y$ and $v = -\partial\psi/\partial x$.

The equations governing the evolution of the functions $f(\eta, \tau)$ and $\theta(\eta, \tau)$ can be obtained by substituting expressions (5) into the governing Equations (1)–(3). It is found that these functions satisfy the following pair of coupled equations:

$$\frac{\partial^2 f}{\partial \eta^2} - \eta \frac{\partial \theta}{\partial \eta} + \theta = 2\tau \frac{\partial \theta}{\partial \tau}, \tag{7}$$

$$\frac{\partial^2 \theta}{\partial \eta^2} + \left(f - 2\tau \frac{\partial f}{\partial \tau}\right)\frac{\partial \theta}{\partial \eta} - \theta \frac{\partial f}{\partial \eta} = \left(1 - 2\tau \frac{\partial f}{\partial \eta}\right)\frac{\partial \theta}{\partial \tau}, \tag{8}$$

which are to be solved for $\tau > 0$, subject to the boundary conditions

$$\begin{aligned} &f(0, \tau) = 0, \quad \frac{\partial \theta}{\partial \eta}(0, \tau) = -\frac{q_2''}{q_1''}, \\ &\frac{\partial f}{\partial \eta}(\infty, \tau) = 0, \quad \theta(\infty, \tau) = 0. \end{aligned} \tag{9}$$

For the steady transport of energy at $\tau = 0$ we write $f(\eta, 0) = f_0(\eta)$ and $\theta(\eta, 0) = \theta_0(\eta)$, say, so that the functions $f_0(\eta)$ and $\theta_0(\eta)$ are the solutions of the coupled ordinary differential equations

$$f_0'' - \eta\theta_0' + \theta_0 = 0, \tag{10}$$

$$\theta_0'' + f_0\theta_0' - f_0'\theta_0 = 0, \tag{11}$$

where prime denotes differentiation with respect to η. The associated boundary conditions (9) reduce to

$$f_0(0) = 0, \quad \theta_0'(0) = -1, \quad f_0'(\infty) = 0, \quad \theta_0(\infty) = 0. \tag{12}$$

At large times, $\tau \to \infty$, the profiles for the nondimensional streamfunction $f(\eta, \tau)$ and the temperature function $\theta(\eta, \tau)$ are known to approach steady state solutions $f(\eta, \infty) = f_\infty(\eta)$ and $\theta(\eta, \infty) = \theta_\infty(\eta)$, respectively, associated with the uniform heat flux q_2'' at the horizontal surface. The functions $f_\infty(\eta)$ and $\theta_\infty(\eta)$ satisfy a pair of coupled ordinary differential equations of precisely the same form as Equations (10) and (11) and are subject to boundary conditions similar to expression (12) with the modification that $\theta_\infty'(0) = -R$, where $R = q_2''/q_1''$. The solution to this system can be recovered as a similarity solution of the original system (10)–(12) so that the functions

$$f_\infty(\eta) = R^{1/4} f_0(\eta R^{1/4}), \quad \theta_\infty(\eta) = R^{3/4}\theta_0(\eta R^{1/4}) \tag{13}$$

represent the final steady state profiles of the streamfunction and temperature function, respectively.

3. Small Time Solution, $\tau \ll 1$

In common with all problems involving impulsive changes in heat flux or temperature, there is a brief period during which the transient effects are confined to a thin, one-dimensional, unsteady boundary-layer adjacent to the surface whose thickness is very small in comparison to that of the steady boundary-layer at $\tau = 0$. Specifically, for $\tau \ll 1$ there exists an inner boundary-layer, whose evolution is described by Equations (7)–(9), which is entirely contained within the initial steady boundary-layer profile, in which the streamfunction and temperature attain their steady state values f_0 and θ_0, respectively. This suggests that to obtain a solution at small times, for which the appropriate length scale is the diffusion scale $\tau^{1/2}$, the boundary-layer equations (7) and (8) have to be transformed by writing

$$f(\eta, \tau) = \tau^{1/2} F(\xi, \tau), \quad \theta(\eta, \tau) = \tau^{1/2} G(\xi, \tau), \quad \xi = \frac{\eta}{2\tau^{1/2}}. \tag{14}$$

Substituting these expressions into Equations (7) and (8) yields the coupled partial differential equations

$$\frac{1}{4}\frac{\partial^2 F}{\partial \xi^2} = 2\tau^{3/2}\frac{\partial G}{\partial \tau}, \tag{15}$$

$$\frac{1}{4}\frac{\partial^2 G}{\partial \xi^2} - \frac{1}{2}G + \left(\frac{1}{2}\xi - \tau^2\frac{\partial F}{\partial \tau}\right)\frac{\partial G}{\partial \xi} = \tau\left(1 - \tau\frac{\partial F}{\partial \xi}\right)\frac{\partial G}{\partial \tau}, \tag{16}$$

which have to be solved subject to the boundary conditions at the plate:

$$F(0, \tau) = 0, \quad \frac{\partial G}{\partial \xi}(0, \tau) = -2R. \tag{17}$$

The solution in this growing inner layer is taken to match with that of the outer steady boundary-layer, which at small η can be approximated by series expansions about $\eta = 0$ of the form

$$f_0(\eta) = a\eta - \tfrac{1}{2}b\eta^2 + \tfrac{1}{24}ab\eta^4 + \mathrm{O}(\eta^5), \tag{18}$$

$$\theta_0(\eta) = b - \eta + \tfrac{1}{2}ab\eta^2 - \tfrac{1}{6}b^2\eta^3 + \mathrm{O}(\eta^4), \tag{19}$$

where $a = f_0'(0) = 1.26286$ and $b = \theta_0(0) = 0.82325$. It follows, by substitution of the transformation (20) into Equations (18) and (19), that for large values of ξ the functions F and G may be expressed as

$$F(\xi, \tau) \sim 2a\xi - 2b\xi^2\tau^{1/2} + \tfrac{2}{3}ab\xi^4\tau^{3/2} + \mathrm{O}(\tau^2), \tag{20}$$

$$G(\xi, \tau) \sim b\tau^{-1/2} - 2\xi + 2ab\xi^2\tau^{1/2} - \tfrac{4}{3}b^2\xi^3\tau + \mathrm{O}(\tau^{3/2}). \tag{21}$$

The behaviour of the inner boundary-layer solution as $\xi \to \infty$ is to be matched with the steady outer solutions (20) and (21). It is the form of these asymptotic expressions which suggests the appropriate perturbation expansion for $\tau \ll 1$ as

$$F(\xi, \tau) = F_0(\xi) + \tau^{1/2}F_1(\xi) + \tau F_2(\xi) + \tau^{3/2}F_3(\xi) + \mathrm{O}(\tau^2), \tag{22}$$

$$G(\xi, \tau) = \tau^{-1/2}G_0(\xi) + G_1(\xi) + \tau^{1/2}G_2(\xi) + \tau G_3(\xi) + \mathrm{O}(\tau^{3/2}). \tag{23}$$

Substitution of these series into Equations (15) and (16) and equating the terms of the same powers of τ gives rise to systems of ordinary differential equations from which closed form solutions for F_i and G_i, where $i = 0, 1, 2, 3$, can be obtained. The resulting expressions for the small time velocity, $\partial F/\partial\xi$, and temperature, G, profiles may be readily established as

$$\frac{\partial F}{\partial \xi} = 2a - 4b\xi\tau^{1/2} + \frac{8}{3}ab\xi^3\tau^{3/2} + \mathrm{O}(\tau^2), \tag{24}$$

$$\begin{aligned} G \;=\; & b\tau^{-1/2} - 2\xi + 2(1 - R)\left(\xi \operatorname{erfc}\xi - \frac{1}{\sqrt{\pi}}\mathrm{e}^{-\xi^2}\right) + \\ & + 2ab\xi^2\tau^{1/2} - \frac{4}{3}b^2\xi^3\tau + \mathrm{O}(\tau^{3/2}), \end{aligned} \tag{25}$$

where $\operatorname{erfc}\xi = (2/\sqrt{\pi})\int_\xi^\infty \mathrm{e}^{-t^2}\mathrm{d}t$ is the complementary error function.

Expressions (24) and (25) are applicable only to the development of the free convection flow in the inner boundary-layer region, that is for $\eta \ll 1$. The velocity and temperature functions which are valid for all values of η are as follows:

$$\frac{\partial f}{\partial \eta}(\eta, \tau) = \frac{\mathrm{d}f_0}{\mathrm{d}\eta}(\eta) + \mathrm{O}(\tau^2), \tag{26}$$

$$\theta(\eta, \tau) = \theta_0(\eta) + (1 - R)\left[\eta \operatorname{erfc}\left(\frac{\eta}{2\tau^{1/2}}\right) - \frac{2}{\sqrt{\pi}}\tau^{1/2}\mathrm{e}^{-\eta^2/4\tau}\right] + \mathrm{O}(\tau^2), \quad (27)$$

at small times τ.

An important physical quantity is the nondimensional temperature on the plate and at small times this function has the following explicit series expansion:

$$\theta_w(\tau) = \theta(0, \tau) = b - \frac{2}{\sqrt{\pi}}(1 - R)\tau^{1/2} + \mathrm{O}(\tau^2). \quad (28)$$

4. Numerical Techniques

Initially the transient effects due to the change in the heat flux at the horizontal plate are confined to a thin fluid region near to the surface and are described by the small time solution. These effects continue to penetrate outwards through the initial boundary-layer and eventually evolve into a new steady state flow. In order to match these small and large time solutions, we now develop a numerical solution of the full boundary-layer equations (1)–(3) by initially using the formulation (15) and (16) in terms of ξ, τ and subsequently the nondimensional partial differential equations (7) and (8) in terms of η, τ.

The evolution of the pairs of interrelated functions F, G and f, θ are separately governed by the pairs of coupled partial differential equations (15), (16) and (7), (8), respectively, which are each parabolic and can be integrated numerically using a step-by-step method similar to that described by Merkin (1972), provided that the coefficients of the corresponding terms $\partial G/\partial\tau$ and $\partial\theta/\partial\tau$ remain positive throughout the solution domain. This marching method enables the solution described by the functions $f_0(\eta)$, $\theta_0(\eta)$ at time $\tau = 0$ to proceed in time and gives a complete solution for $\tau \leqslant \tau_n^*$, where τ_n^* is the maximum value of τ reached in the forward integrating numerical scheme, which is less than the precise time τ_{p}^* satisfying

$$\tau_{\mathrm{p}}^* \frac{\partial F}{\partial \xi}(0, \tau_{\mathrm{p}}^*) = 2\tau_{\mathrm{p}}^* \frac{\partial f}{\partial \eta}(0, \tau_{\mathrm{p}}^*) = 1. \quad (29)$$

The application of the step-by-step scheme to the pair of coupled equations (15) and (16) enables the accurate evolution of the temperature and velocity profiles to be determined over a developing inner layer whose width increases with time. If ξ_∞ and η_∞ are interpreted as being finite values of the spatial variables at which the associated boundary conditions are to be applied, then at the exact time $\tilde{\tau}_{\mathrm{p}} = (\eta_\infty/2\xi_\infty)^2$ we must transfer to the step-by-step scheme applied to Equations (7) and (8). We again adopt the notation $\tilde{\tau}_n$ to denote the corresponding value of τ which is reached in our numerical techniques.

At the time $\tau = \tau_n^*$ the forward integration approach breaks down and the coefficients of $\partial G/\partial\tau$ and $\partial\theta/\partial\tau$ in the governing Equations (16) and (8), respectively, are tending towards negative values at the surface of the horizontal plate. Based

upon the profiles $f(\eta, \tau_n^*)$ and $\theta(\eta, \tau_n^*)$ at this time and the asymptotic steady state profiles $f_\infty(\eta)$ and $\theta_\infty(\eta)$, defined in Equation (13), we attempt to complete the numerical integration and derive a solution over $\tau_n^* < \tau < \infty$ by adopting a matching approach in Section 4.3.

4.1. NUMERICAL SOLUTION FOR $0 < \tau \leqslant \tilde{\tau}_n$

In order to evaluate accurately the initial evolution of both the nondimensional fluid velocity $\partial f/\partial \eta$ and the nondimensional fluid temperature θ we apply the direct, forward integration scheme to Equations (15) and (16) and begin the numerical solution at the small time $\tau = \tau_0 > 0$. Thus, the governing pair of coupled equations (15) and (16) must be solved subject to the boundary conditions (17), the initial profiles

$$F(\xi, \tau_0) \approx 2a\xi - 2b\xi^2\tau_0^{1/2} + \frac{2}{3}ab\xi^4\tau_0^{3/2}, \tag{30}$$

$$G(\xi, \tau_0) \approx b\tau_0^{-1/2} - 2\xi + 2(1-R)\left[\xi \operatorname{erfc}\xi - \frac{1}{\sqrt{\pi}}e^{-\xi^2}\right] + \\ +2ab\xi^2\tau_0^{1/2} - \frac{4}{3}b^2\xi^3\tau_0, \tag{31}$$

which follow from the small time analysis, and the following conditions:

$$F(\xi_\infty, \tau) = \tau^{-1/2} f_0\left(2\sqrt{\tau}\xi_\infty\right), \qquad G(\xi_\infty, \tau) = \tau^{-1/2}\theta_0(2\sqrt{\tau}\xi_\infty), \tag{32}$$

where the undisturbed states $f_0(\eta)$ and $\theta_0(\eta)$, following from the initial steady solution, remain.

The finite spatial domain is divided into N^ξ grid spacings of length $h^\xi = \xi_\infty/N^\xi$ and a variable time step is used, with the time step at the start of the jth time increment being denoted by $\Delta\tau_j$. We also introduce the notation $F_{i,j}$ and $G_{i,j}$ to represent the finite-difference approximations to the nondimensional streamfunction F and temperature function G, respectively, at the point $\xi = (i-1)h^\xi$ for some time $\tau = \tau_j$.

Given a complete solution $F_{i,j}$, $G_{i,j}$, $i = 1, \ldots, N^\xi + 1$, at time τ_j we require the solution for $F_{i,j+1}$, $G_{i,j+1}$ at the next time $\tau = \tau_{j+1} = \tau_j + \Delta\tau_j$ and adopt the step-by-step finite-difference procedure similar to that described by Merkin (1972). This numerical formulation is very well described by Haris *et al.* (1997a) and we will not present it here.

Consider the system of linear algebraic equations $\mathcal{G}_k^1 = 0$ and the system of nonlinear algebraic equations $\mathcal{G}_k^2 = 0$ resulting from the finite-difference approximations to the governing equations (15) and (16), respectively. Given initial approximations to the solutions of these systems, it would be natural to assume that an iterative approach could be utilised to successively determine better approximations by employing Newton's method and alternately inverting the linear system

associated with $\mathcal{G}_k^1$ or $\mathcal{G}_k^2$ using the Thomas algorithm for tri-diagonal matrices. This approach was attempted and found to be successful initially, but ultimately did not lead to a convergent solution after a short time interval. It was found that a convergent solution at each time step could only be guaranteed for $\tau \leqslant \tilde{\tau}_n$ provided that the systems $\mathcal{G}_k^1$ and $\mathcal{G}_k^2$ were combined to produce a single system $\mathcal{G}_k = 0$ of nonlinear algebraic equations which must be solved directly to determine the values of the unknowns $F_{2,j+1}, \ldots, F_{N^\xi,j+1}$ and $G_{1,j+1}, \ldots, G_{N^\xi,j+1}$ simultaneously. To solve the nonlinear system of algebraic equations $\mathcal{G}_k = 0$ we utilise the NAG routine C05PDF.

To accurately describe the initial evolution, the time increment $\Delta\tau_0$ at time $\tau = \tau_0$ is set to some prescribed small value and subsequently a time step doubling procedure is adopted to reduce the computations at later times.

4.2. NUMERICAL SOLUTION FOR $\tilde{\tau}_n < \tau \leqslant \tau_n^*$

As noted earlier, the restrictions to finite dimensional ξ and η spaces enable us to transfer from the forward integrating solution procedure of Section 4.1 in ξ, τ variables to the corresponding version of the same approach in η, τ variables at the precise time $\tilde{\tau}_\mathrm{p} = (\eta_\infty/2\xi_\infty)^2$. Based upon the streamfunction and temperature profiles at the final time $\tilde{\tau}_n$ reached in the numerical solution of the previous section, we can now continue the step-by-step method, using a technique similar to that described by Merkin (1972), towards the time τ_p^* predicted by Equation (29).

The full boundary-layer equations (7) and (8) are now solved subject to the boundary conditions (9) and the initial profiles

$$f(\eta, \tilde{\tau}_n) = \tilde{\tau}_n^{1/2} F(\xi, \tilde{\tau}_n)\Big|_{\xi=\eta/2\tilde{\tau}_n^{1/2}}, \qquad \theta(\eta, \tilde{\tau}_n) = \tilde{\tau}_n^{1/2} G(\xi, \tilde{\tau}_n)\Big|_{\xi=\eta/2\tilde{\tau}_n^{1/2}}, \tag{33}$$

where the conditions valid for $\eta \to \infty$ are applied at $\eta = \eta_\infty = 2\xi_\infty \tilde{\tau}_n^{1/2}$, by employing the numerical formulation used in the paper by Harris *et al.* (1997a).

The resulting system of nonlinear algebraic equations $\mathcal{G}_k = 0$ can now be solved to simultaneously determine the values of f and θ at the next time step using the NAG routine C05PDF, as in Section 4.1, based upon the initial profiles (33).

4.3. NUMERICAL SOLUTION FOR $\tau_n^* < \tau < \infty$

At large times the solutions for the nondimensional streamfunction $f(\eta, \tau)$ and the temperature function $\theta(\eta, \tau)$ are known to approach the steady state similarity solution profiles $f_\infty(\eta)$ and $\theta_\infty(\eta)$, respectively, associated with the uniform heat flux q_2'' at the horizontal plate surface, as derived in Equation (13). We must now attempt to characterise the evolution of the profiles reached at time τ_n^*, when the numerical techniques of Sections 4.1 and 4.2 terminate, towards these final steady state profiles.

The matching technique originated by Dennis (1972) has been successfully applied by the present authors to some related problems of impulsive changes in uniform surface heat flux or temperature on vertical plates, see Harris *et al.* (1997a, b, 1998) wherein comprehensive details of this iterative approach are presented. In the finite-difference approximation to Equation (8) we replace $\partial\theta/\partial\tau$ by either a backward or a forward difference depending on whether the coefficient of $\partial\theta/\partial\tau$ is positive or negative, respectively, to attempt to achieve a convergent solution using standard iterative techniques.

It was deduced for the forward integration approach that ensuring convergence of the solution of the governing boundary-layer equations (7) and (8) crucially depends on solving for the unknown values of the nondimensional streamfunction and temperature simultaneously. In view of this, an extension of the above method is attempted in which tri-diagonal systems for $f(\eta, \tau)$ and $\theta(\eta, \tau)$ are each set up along lines of constant τ within the grid and solved alternately to derive new estimates for $f(\eta, \tau)$ and $\theta(\eta, \tau)$, using the Thomas algorithm for tri-diagonal matrices. The further extension to solving for both $f(\eta, \tau)$ and $\theta(\eta, \tau)$ simultaneously along a line of constant τ by constructing an associated system of nonlinear algebraic equations would again require the implementation of the NAG routine C05PDF, as in Sections 4.1 and 4.2, and clearly require a significant amount of computational time per iteration through the grid for a suitable value of τ_∞. This further extension has therefore not been attempted.

5. Results

The NAG routine D02HAF was used to solve the coupled ordinary differential equations (10) and (11), subject to the boundary conditions (12). In this numerical procedure an absolute error tolerance must be supplied and the upper range of integration must be specified at some finite value instead of infinity. In all the results presented in this paper a tolerance of 10^{-8} and an endpoint of $\eta = 14$ were used as it was found that any further decrease and increase, respectively, of the values did not produce results which showed further significant variation.

In the discussion of the results which follow we concentrate on the two cases $R = 0.5$ and 2.

5.1. RESULTS FOR $0 < \tau \leqslant \tau_n^*$

The restriction to a finite dimensional ξ space was achieved by taking $\xi_\infty = 12$ and thus the precise time at which transfer to the method of Section 4.2 takes place is $\widetilde{\tau}_\mathrm{p} = 0.34028$, taking $\eta_\infty = 14$. This value of η_∞ was taken to be sufficiently large to ensure that θ and $\partial f/\partial\eta$ are negligible over an interval approaching η_∞ and the results up to $\tau = \tau_n^*$ obtained using larger values of η_∞ show no significant deviation. The value of ξ_∞ was separately increased but again provided no discernible graphical variation. Furthermore, using $\xi_\infty = 12$ the profiles of the

nondimensional temperature and velocity function remained close to their initial steady state values over an interval of the ξ space approaching ξ_∞ for all times up to $\tilde{\tau}_n$, when the transfer to the forward integration method in η, τ takes place, which indicates that ξ_∞ has been specified sufficiently large. For the case $R = 2$, the profile of $f(\eta, \tau)$ was further observed to achieve a small local maximum slightly above the value enforced to occur at the edge of the growing inner boundary-layer. As this may be an indication that the boundary-layer thickness is increasing more rapidly than expected, the value of ξ_∞ was increased, keeping $N^\xi = 200$, but the local maximum in the profile persisted.

The initial time τ_0 and first time increment $\Delta\tau_0$ were assigned the values $\tau_0 = 10^{-5}$ and $\Delta\tau_0 = 10^{-6}$, respectively. Any smaller values of these parameters were found to produce results which are graphically indistinguishable from those presented in the figures and, moreover, the values specified for τ_0 and $\Delta\tau_0$ are consistent with those used by the present authors in related papers (see Harris *et al.*, 1997a, b, 1998). For the ratios $R = 0.5$ and 2, the time step doubling criterion was successful in steadily increasing the time increments and led to a time increment of $\Delta\tau = 2.048 \times 10^{-3}$ at the times $\tau = \tilde{\tau}_n = 0.3367$ and $\tau = \tilde{\tau}_n = 0.3387$, respectively. The numerical values of $\eta_\infty = 2\xi_\infty \tilde{\tau}_n^{1/2}$ were therefore calculated to be $\eta_\infty = 13.9258$ and 13.9681 for $R = 0.5$ and 2, respectively.

The time τ_n^*, denoting the largest value of τ reached in the numerical scheme before τ_{p}^*, defined by Equation (29), was found to be $\tau_n^* \approx 0.4063$ and $\tau_n^* \approx 0.3879$ for $R = 0.5$ and 2, respectively.

The main source of variation in the solutions for the nondimensional fluid temperature $\theta(\eta, \tau) = \tau^{\frac{1}{2}} G(\xi(\eta, \tau), \tau)$ and fluid velocity function

$$\frac{\partial f}{\partial \eta}(\eta, \tau) = \tau^{1/2} \frac{\partial F}{\partial \xi}(\xi(\eta, \tau), \tau)$$

arise by considering changes in the number of grid spaces N^ξ. The values of N^ξ considered here were $N^\xi = 100$ and 200 with corresponding values of $h^\xi = 0.12$ and 0.06. It was observed in these cases that as N^ξ increases, and consequently h^ξ decreases, the initial development of the numerical solution approached that of the small time solution but further refinements of the grid were not possible due to the already considerable computational time required for $N^\xi = 200$. Thus, the value $N^\xi = 200$ has been used in all the results presented in this paper. Furthermore, the number of spatial grid points and final time increment at $\tau = \tilde{\tau}_n$ were continued to the method described in Section 4.2 for $\tilde{\tau}_n < \tau \leqslant \tau_n^*$, so that $N^\eta = 200$ and $h^\eta = \eta_\infty / N^\eta \approx 0.07$. An improvement in the accuracy of the solution was again observed to occur as the spatial grid was refined from $N^\eta = 100$ to $N^\eta = 200$.

Figure 1 shows the variation of the temperature profiles $\theta(\eta, \tau)$ at various times τ calculated for $R = 0.5$ and 2. The steady state solution as predicted by Equations (10) and (11) is also included in this figure. We see that the nondimensional temperature profiles evolve from $\tau = 0$ towards the large time steady state solution although initially the effects of the change in surface heat flux of the plate are not

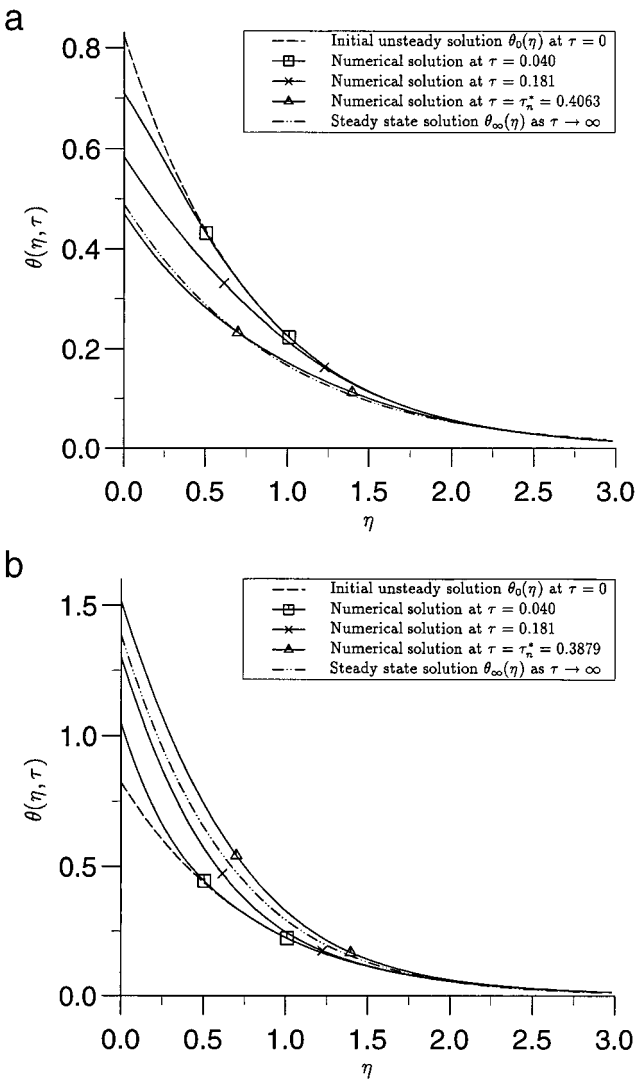

Figure 1. Variation of the nondimensional temperature function $\theta(\eta, \tau)$ as a function of η, shown at various values of τ during the evolution from the initial unsteady state at $\tau = 0$ to the termination of the forward integration approach at $\tau = \tau_n^*$, and the large time solution valid as $\tau \to \infty$: (a) $R = 0.5$; (b) $R = 2$.

felt near the outer edge of the boundary-layer. As time progresses towards $\tau = \tau_n^*$ the effect of the impulsive change in the surface conditions penetrate further into the initial steady state boundary-layer but the profile of the temperature overshoots the large time solution before the step-by-step method breaks down. This observation is further demonstrated in the evolution of the nondimensional plate surface temperature with time τ in Figure 2 where $\theta_w(\tau)$ is found to have both reached a value beyond its predicted steady state value by the time τ_n^* and to be continuing to

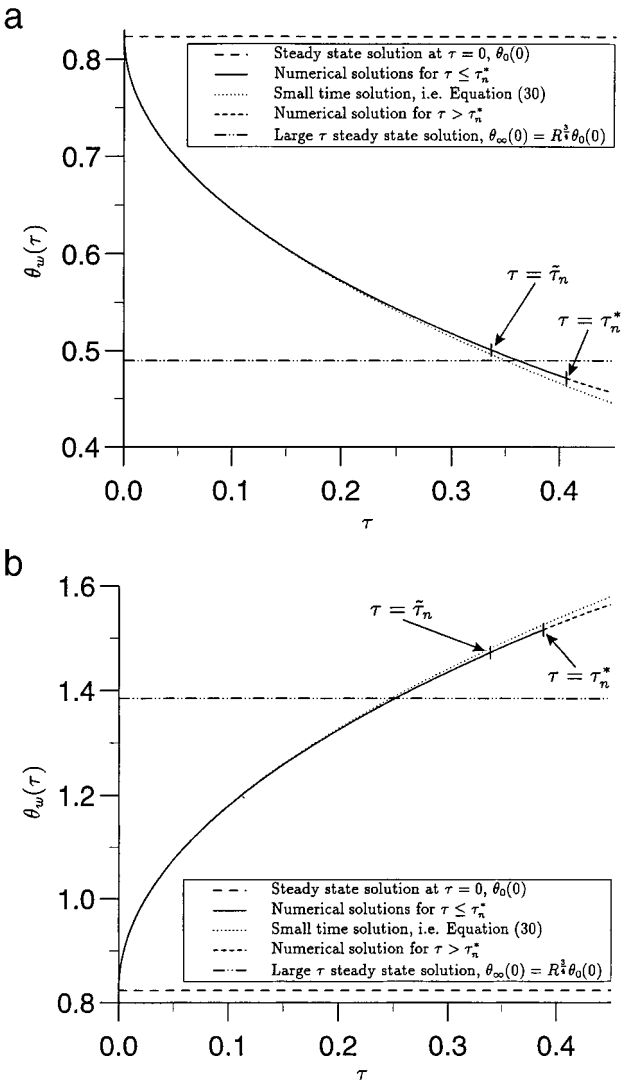

Figure 2. Variation of the nondimensional wall temperature $\theta_w(\tau)$ as a function of τ, the small time solution and the steady state solutions at $\tau = 0$ and as $\tau \to \infty$, where the transition between the solution methods of Sections 4.1 and 4.2 and Sections 4.2 and 4.3 occur at the indicated times $\tilde{\tau}_n$ and τ_n^*, respectively: (a) $R = 0.5$; (b) $R = 2$.

rapidly decrease or increase with time according as to whether $R = 0.5$ or $R = 2$, respectively. The numerical, transient solution is also shown to develop closely following the small time solution (28) and is graphically almost identical when $\tau < 0.15$ for both $R = 0.5$ and 2. As the numerical solution begins to deviate from the small time analytical solution, this truncated series approximation (28) becomes invalid.

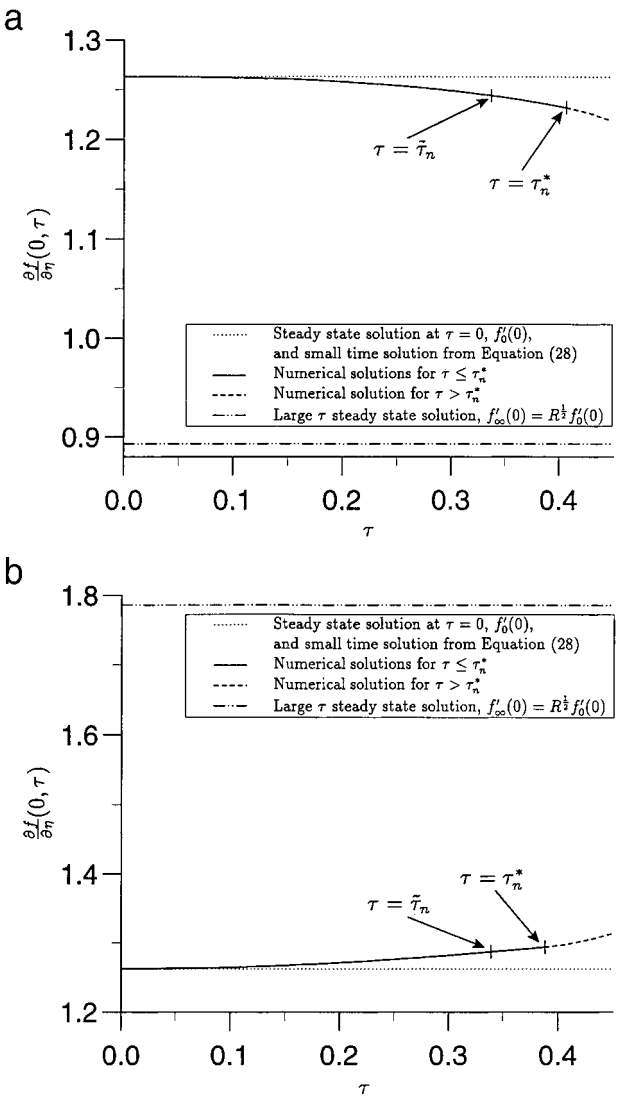

Figure 3. Variation of the nondimensional wall velocity $\partial f(0, \tau)/\partial \eta$ as a function of τ, the small time solution and the steady state solution as $\tau \to \infty$, where the transition between the solution methods of Sections 4.1 and 4.2 and Sections 4.2 and 4.3 occur at the indicated times $\tilde{\tau}_n$ and τ_n^*, respectively. (a) $R = 0.5$; (b) $R = 2$.

The evolution of the nondimensional fluid velocity at the plate surface $\partial f(0, \tau)/\partial \eta$ with time τ is also presented in Figure 3. Again, the transient solution initially follows the constant small time solution predicted in Equation (26), which indicates that the approach of $\partial f(0, \tau)/\partial \eta$ towards its predicted final steady state value is much slower than the corresponding evolution of the plate surface temperature. Furthermore, up to the time τ_n^* at which the forward integration method

terminates, there is an insignificant change in the whole of the $\partial f(\eta, \tau)/\partial \eta$ profile. When viewed graphically, the profiles of the velocity function $\partial f(\eta, \tau)/\partial \eta$ at τ_n^* are almost indistinguishable from the corresponding initial steady state profiles and it is for this reason that the evolution of the velocity profiles, in a similar form to those presented in Figure 1 for $\theta(\eta, \tau)$, are not presented here for the time period over which the forward integration approach is applicable.

5.2. RESULTS FOR $\tau_n^* < \tau < \infty$

The matching technique originated by Dennis (1972) was applied in order to predict the evolution of the known profiles of the temperature and streamfunction reached at the termination of the forward integrating approach of Sections 4.1 and 4.2 towards the predicted large time steady state profiles. This technique was implemented with a constant time increment which was chosen to be almost identical to the spatial step size, as required in Harris *et al.* (1997a, b, 1998). The spatial grid size specified at $\tau = \tau_n^*$, from the termination of the forward integration approach, was continued here so that both an $n = 100$ and an $n = 200$ spatial grid were applied. Although the value $\eta_\infty \approx 14$ has been shown to be valid for $\tau \leqslant \tau_n^*$, this value of η_∞ was additionally extended, with a corresponding increase in n. The final steady state profiles were enforced at various values of τ_∞ up to $\tau_\infty = 20$. In all cases, for $R = 0.5$, the solution diverged rapidly and thus no convergent results could be derived based upon the profiles $f(\eta, \tau_n^*)$ and $\theta(\eta, \tau_n^*)$ specified at $\tau = \tau_n^*$. To attempt a more gradual approach towards the expected solution, an under-relaxation method was employed with a small relaxation parameter but again this approach eventually led to divergence.

In the first extension of the method described here, based upon solving tridiagonal systems for $f(\eta, \tau)$ and $\theta(\eta, \tau)$ along lines of constant τ within the grid, we found that again no convergent solution could be achieved. Furthermore, in a related paper by Ingham *et al.* (1985) the impulsive cooling of a horizontal surface, for which the governing boundary-layer equations have a similar appearance to Equations (7) and (8), was studied and, despite no difficulties occurring for the corresponding problems on vertical surfaces, the method of Dennis (1972) again proved ineffective in matching the small and large time solutions.

At nondimensional times just after τ_n^* the nondimensional velocity near the horizontal surface is such that

$$q(\eta, \tau) = 1 - 2\tau \frac{\partial f}{\partial \eta}(\eta, \tau)$$

is either negative or very small and tending towards a negative value. Figure 4 demonstrates how the profiles of the nondimensional temperature $\theta(\eta, \tau)$ and velocity $\partial f(\eta, \tau)/\partial \eta$ evolve beyond $\tau = \tau_n^*$, for $R = 0.5$, using an approach in which we set the term $q(\eta, \tau) \equiv 0$ at all points for which it is negative. The profiles of nondimensional temperature are observed to continue to decrease with nondimensional time until a minimum profile is reached at around $\tau = 2$. The profile

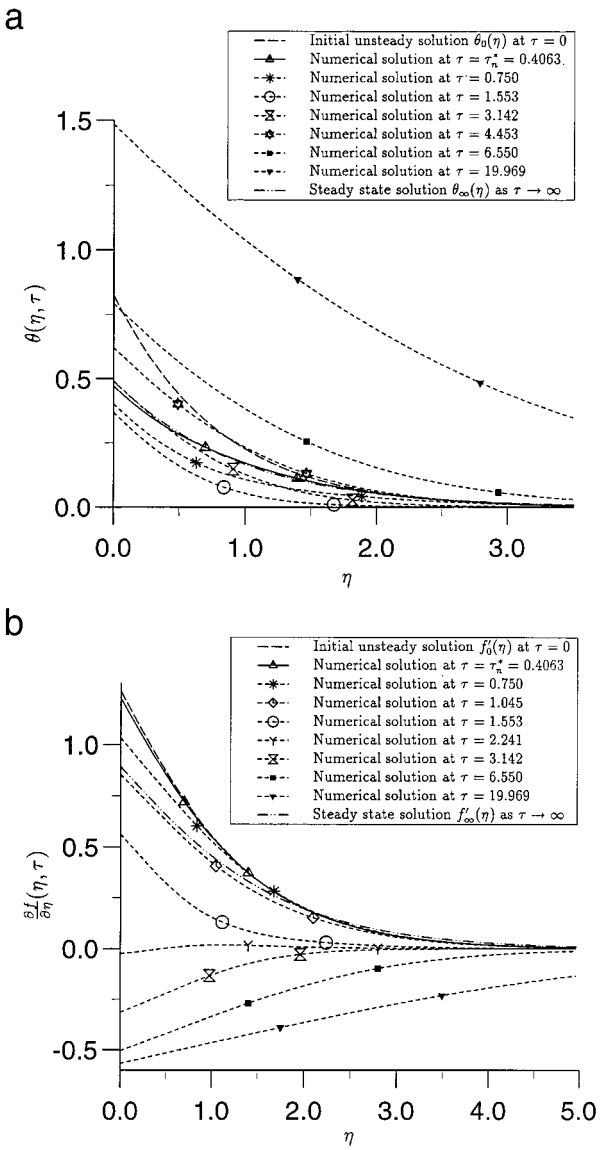

Figure 4. Variation of the solution profiles with η, showing the evolution from the valid solutions at $\tau = \tau_n^*$ determined using the technique in which we set $q \equiv 0$ whenever it becomes negative, together with the initial unsteady state at $\tau = 0$ and the large time solution valid as $\tau \to \infty$, for the case $R = 0.5$. (a) Profiles of the nondimensional temperature function $\theta(\eta, \tau)$; (b) Profiles of the nondimensional velocity function $\partial f(\eta, \tau)/\partial \eta$.

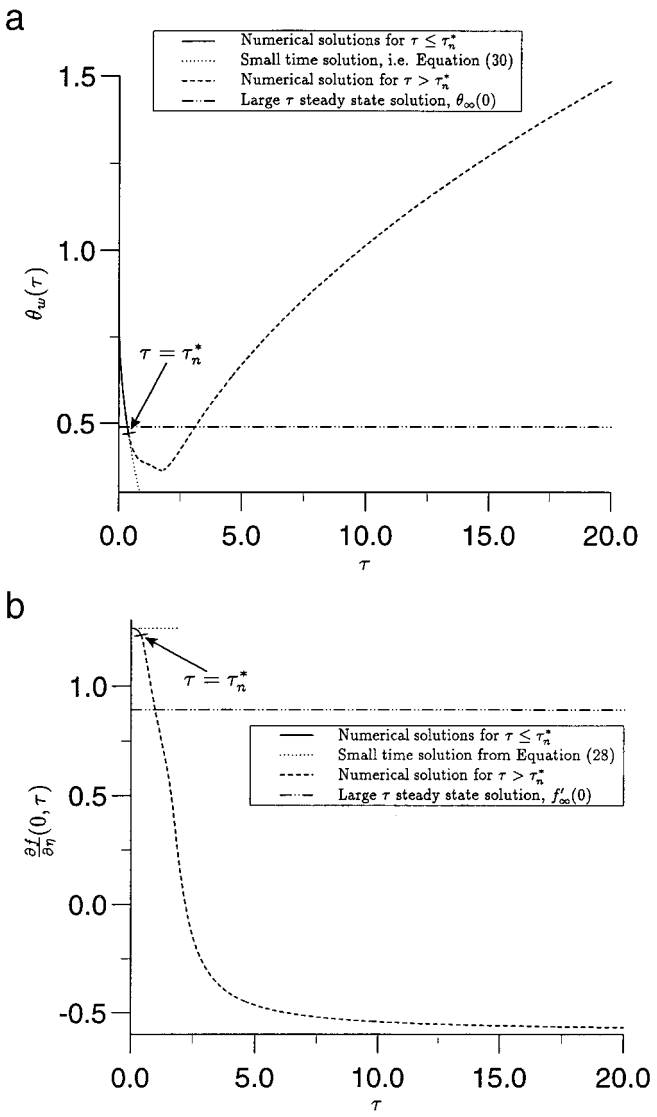

Figure 5. The evolution with τ from the valid solutions at $\tau = \tau_n^*$, using the technique in which we set $q \equiv 0$ whenever it becomes negative, together with the small time solution and the large time solution valid as $\tau \to \infty$, for the case $R = 0.5$. (a) The nondimensional wall temperature $\theta_w(\tau)$; (b) The nondimensional wall velocity $\partial f(0, \tau)/\partial \eta$.

then begins to increase throughout and passes over the predicted large time steady state profile. The profile continues to grow with the value of the nondimensional temperature becoming significantly above zero at the edge of the spatial domain. The boundary-layer grows in size until the numerical solution technique fails to converge at some time beyond about $\tau = 20$. The same growth in the boundary-layer thickness is observed in the evolution of the nondimensional velocity function

profiles. These profiles are again seen to initially evolve such that the change in the surface heat flux does not affect the velocity function near the outer edge of the boundary-layer before the solution overshoots the predicted large time steady state profile and continues to decrease for all values of η, eventually becoming negative throughout the spatial domain $0 \leqslant \eta \leqslant \eta_\infty$. Clearly the term $q(\eta, \tau)$ has become positive throughout the domain again as time increases and we return to solving the original finite-difference equations, namely those described in Section 4.2. To demonstrate further the above behaviour, the evolution of the nondimensional surface temperature $\theta_w(\tau)$ and velocity on the surface $\partial f(0, \tau)/\partial \eta$ are presented in Figure 5. Thus, rather than approaching steady state values, the solutions discussed here continue to remain highly transient at large times and the right-hand sides of the governing boundary-layer equations (7) and (8) do not become small. Figure 5(b) shows that the velocity on the surface becomes negative when τ is large and hence reversed flows have been detected. Clearly, the numerical scheme is inappropriate at such times as the flow of information in this parabolic equation is in the wrong direction. This clearly illustrates that this matching approach has failed.

Setting the term $q(\eta, \tau) \equiv 0$ at all points where it is negative for the case of $R = 2$ did not allow a valid solution to be reached very far beyond τ_n^*. Instead, an oscillatory behaviour soon developed and the technique failed to converge. To ensure that these oscillations were not due to increasing errors arising from the local maximum in the profile of $f(\eta, \tau)$ observed in Section 5.1, the forward integration approach using the (η, τ) variables defined in Section 4.2 was begun at the initial time τ_0 using the small time approximation, as described for the method of Section 4.1. Exactly the same characteristic oscillations were found to arise at a similar time beyond τ_n^*.

6. Conclusions

The transient free convection from a horizontal flat surface, embedded in a fluid-saturated porous medium, which develops due to a sudden change in the surface heating rate has been analysed thoroughly. An analytical solution which is valid for small times and a large time numerical similarity solution profile have been obtained for some values of the physical parameter R, representing the ratio of the final surface heat flux to the initial surface heat flux. The cases of $R = 0.5$ and $R = 2$ considered here are representative of the two possible cases of a decrease and increase in the surface heating rate, respectively. It has been shown that the small time transient is initially confined within the established boundary-layer region near the surface, corresponding to the initial heating situation. Later, convection effects modify the solution at a greater distance from the horizontal surface.

A numerical solution of the full boundary-layer equations has been obtained using a forward integration technique and the results have been validated against the small time analytical solution. However, a time is reached at which this march-

ing approach is no longer well posed and beyond this time we have not been able to continue the transient solution towards the large time temperature and velocity profiles. This difficulty was found to arise due to the change in sign of the time derivative term within one of the governing boundary-layer equations. The failure to match the small and large time solutions therefore makes the present problem somewhat distinct from related transient convection problems on vertical surfaces, arising due to impulsive changes in surface heat flux or temperature, for which no such difficulties have been reported. Consequently, the question of whether or not it is possible to reach the predicted large time regime based upon the initial conditions posed here remains unresolved.

Work is now in progress to investigate other possible large time solutions and on performing a linear stability analysis on the steady state solutions. These investigations should provide further insights into this very interesting problem.

Acknowledgements

Two of the authors, D.B. Ingham and I. Pop, gratefully acknowledge some financial support from The Royal Society.

References

Chang, I. D. and Cheng, P.: 1983, Matched asymptotic expansions for free convection about an impermeable horizontal surface in a porous medium, *Int. J. Heat Mass Transfer* **26**, 163–174.

Chaudhary, M. A., Merkin, J. H. and Pop, I.: 1996, Natural convection from a horizontal permeable surface in a porous medium – numerical and asymptotic solutions, *Transport in Porous Media* **22**, 327–344.

Cheng, P. and Chang, I. D.: 1976, Buoyancy induced flows in a saturated porous medium adjacent to impermeable horizontal surfaces, *Int. J. Heat Mass Transfer* **19**, 1267–1272.

Dennis, S. C. R.: 1972, The motion of a viscous fluid past an impulsively started semi-infinite flat plate, *J. Inst. Math. Appl.* **10**, 105–117.

Harris, S. D., Ingham, D. B. and Pop, I.: 1996, Transient free convection on a vertical plate subjected to a change in surface heat flux in porous media, *Fluid Dynam. Res.* **18**, 313–324.

Harris, S. D., Ingham, D. B. and Pop, I.: 1997a, Free convection from a vertical plate in a porous medium subjected to a sudden change in surface heat flux, *Transport in Porous Media* **26**, 207–226.

Harris, S. D., Ingham, D. B. and Pop, I.: 1997b, Free convection from a vertical plate in a porous media subjected to a sudden change in surface temperature, *Int. Comm. Heat Mass Transfer* **24**, 543–552.

Harris, S. D., Elliott, L., Ingham, D. B. and Pop, I.: 1998, Transient free convection flow past a vertical flat plate subjected to a sudden change in surface temperature, *Int. J. Heat Mass Transfer* **41**, 357–372.

Higuera, F. J.: 1997, Conjugate natural convection heat transfer between two porous media separated by a horizontal wall, *Int. J. Heat Mass Transfer* **40**, 3157–3161.

Higuera, F. J. and Weidman, P. D.: 1995, Natural convection beneath a downward facing heated plate in a porous medium, *Euro. J. Mech. B/Fluids* **14**, 29–40.

Ingham, D. B. and Pop, I. (eds): 1998, *Transport Phenomena in Porous Media*, Elsevier, Oxford.

Ingham, D. B., Merkin, J. H. and Pop, I.: 1985, Flow past a suddenly cooled horizontal flat surface in a saturated porous medium, *Acta Mechanica* **56**, 205–217.

Johnson, C. H. and Cheng, P.: 1978, Possible similarity solutions for free convection boundary layers adjacent to flat plates in porous media, *Int. J. Heat Mass Transfer* **21**, 709–718.

Lesnic, D., Ingham, D. B. and Pop, I.: 1995, Conjugate free convection from a horizontal surface in a porous medium, *J. Appl. Math. Mech. (ZAMM)* **75**, 715–722.

Merkin, J. H.: 1972, Free convection with blowing and suction, *Int. J. Heat Mass Transfer* **15**, 989–999.

Merkin, J. H. and Zhang, G.: 1990, On the similarity solutions for free convection in a saturated porous medium adjacent to impermeable horizontal surfaces, *Wärme- und Stoffübertr.* **25**, 179–184.

Nakayama, A.: 1995, *PC-Aided Numerical Heat Transfer and Convective Flow*, CRC Press, Tokyo.

Nield, D. A. and Bejan, A.: 1999, *Convection in Porous Media*, 2nd edn, Springer-Verlag, New York.

Pop, I. and Cheng, P.: 1983, The growth of a thermal layer in a porous medium adjacent to a suddenly heated semi-infinite horizontal surface, *Int. J. Heat Mass Transfer* **26**, 1574–1576.

Rees, D. A. S.: 1996, The effect of inertia on free convection from a horizontal surface embedded in a porous medium, *Int. J. Heat Mass Transfer* **39**, 3425–3430.